Institute of Paper Science and Technology
Atlanta, Georgia

IPST TECHNICAL PAPER SERIES

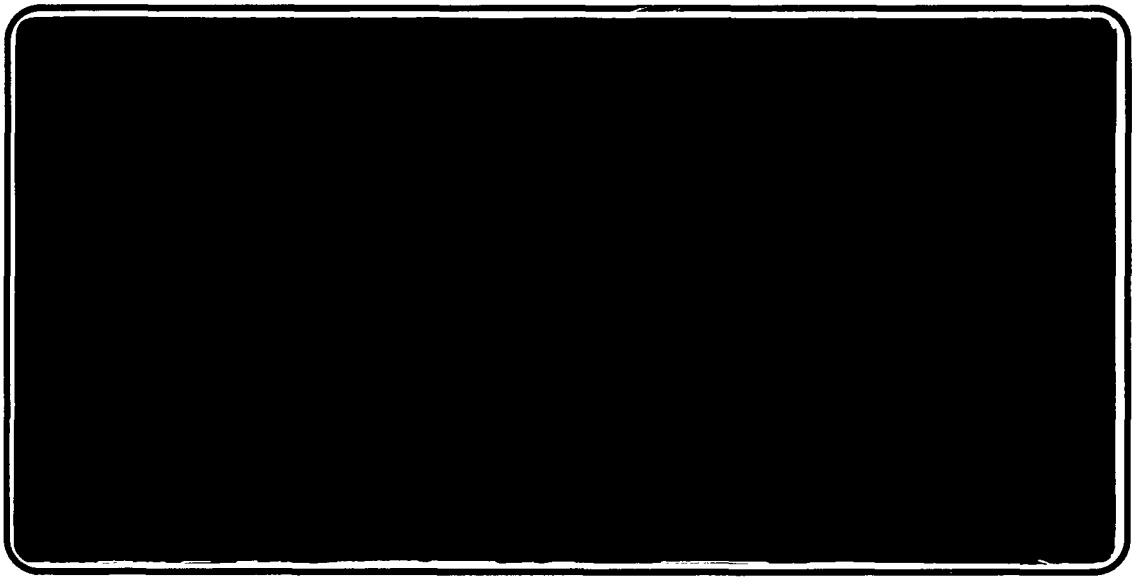

NUMBER 378

MECHANISMS OF LIQUID SHEET BREAKUP AND THE RESULTING DROPLET SIZE DISTRIBUTIONS

T.M. SPIELBAUER AND C.K. AIDUN

MAY, 1991

Mechanisms of Liquid Sheet Breakup and the Resulting Droplet Size Distributions

T.M. Spielbauer and C.K. Aidun

Submitted for
Tappi Journal

MECHANISMS OF LIQUID SHEET BREAKUP AND THE RESULTING DROPLET SIZE DISTRIBUTIONS

T.M. Spielbauer
Graduate Student
Institute of Paper Science
and Technology
575 14th St., NW
Atlanta, GA 30318

C.K. Aidun
Assistant Professor of Engineering
Institute of Paper Science
and Technology
575 14th St., NW
Atlanta, GA 30318

EXECUTIVE SUMMARY

One variable available for use in controlling recovery boiler operation is the black liquor delivery system. The initial droplet size distribution is expected to affect capacity, emissions and safety. In order to use this parameter effectively, the hydrodynamic mechanisms involved in the spraying process must be understood. With this knowledge it is hoped that nozzle geometry and operating conditions can be manipulated to improve boiler performance.

In this paper, the various steps in the production of droplets from a sheet of fluid are reviewed. The results are then used to predict typical droplet size distributions.

NOTATION

symbol	definition
A	surface area
A_o	cross-sectional area of a fan spray nozzle
D_o	nozzle orifice diameter
e	rim velocity ($\delta r_p/\delta t$)
e_0	rim velocity corrected to zeroth order for sheet thickness
e_1	rim velocity corrected to first order in sheet thickness
h_o	unperturbed half sheet thickness
h_x	half sheet thickness at a position, x, downstream
H	magnitude of a perturbation to the sheet interface position
h_+	upper perturbed sheet surface position
h_-	lower perturbed sheet surface position
i	$\sqrt{-1}$
j	phase subscript (j=l, liquid; j=g, gas)
k	spatial perturbation wave number ($k=2\pi/\lambda$)
k_{max}	wave number of the optimum disturbance at breakup
k_o	geometric nozzle parameter
K_j	constant in the unsteady Bernoulli Equation for phase j
L	length of a perforation rim
L_{tot}	total length of all group q perforation rims
m_o	mass flow rate through a swirl cone nozzle
N_p	number of perforations
N_d	number of droplets
n	tangential perturbation wave number
P	pressure
r	strand radius
r_o	initial strand radius
r_p	perforation radius
r_x	perforation radius at position x
R	radius of curvature
R_o	distance from nozzle to center of perforation
s	growth rate parameter
s_r	real part of the growth rate parameter
s_i	imaginary part of the growth rate parameter
t	time
U_o	velocity at orifice exit
U_s	mean free sheet velocity
V	gas velocity relative to the liquid surface
$\underline{v}_j$	velocity vector for phase j
v_x	velocity component normal to the center line of the sheet
v_z	velocity component tangent to the center line of the sheet
x	radial position measured from the point of sheet formation
x_t	radial position of the tip of a splash plate
x_v	radial position at which viscous forces begin on a plate
z	radial distance in a strand/out-of-plane distance in a sheet

I_n	modified Bessel function of the first kind, of order n
K_n	modified Bessel function of the second kind, of order n
Re_j	$\rho_l U D_o/\mu_l$, Reynolds Number (based on liquid properties, jet diameter)
Re_r	$\rho_l U r_o/\mu_l$, Reynolds Number (based on liquid properties, strand radius)
We_h	$\rho_l U^2 h_x/2\sigma$, Weber Number (based on liquid properties, sheet thickness)
We_r	$\rho_l U^2 r_o/\sigma$, Weber Number (based on liquid properties, strand radius)

α	spread angle of a sheet
β	swirl cone spray angle
β_o	cone angle at the nozzle orifice
φ_j	velocity potential for phase j
Φ_j	magnitude of a disturbance to the velocity potential
γ	density ratio (ρ_g/ρ_l)
η	disturbance magnitude
λ	wavelength of a disturbance
λ_c	minimum unstable sheet disturbance wavelength
λ_{opt}	optimum sheet disturbance wavelength
λ_{max}	wavelength of the optimum disturbance at breakup
μ_g	gas phase viscosity
μ_l	liquid phase viscosity
π	3.14159...
θ	azimuthal polar coordinate
ρ_g	density of the gas phase
ρ_l	density of the liquid phase
σ	surface tension
ξ	dimensionless wave number
ψ	dimensionless growth rate parameter
ζ	phase angle between the disturbances to upper and lower sheet surfaces

ABSTRACT

Both a wave and a perforation mechanism have been proposed as the first step in the breakup of fluid sheets. Analytical analyses of these processes are reviewed. As both mechanisms produce cylindrical strands which subsequently break up to form droplets, jet breakup analyses are reviewed as well. By combining the sheet and strand breakup results, it will be shown that a discrete number of droplet sizes is predicted from the wave mechanism, while the perforation mechanism can be used to predict a distribution of droplet sizes similar to that observed experimentally.

KEYWORDS: droplet size distribution, fluid mechanics, hydrodynamic stability, jet breakup, perforation mechanism, sheet breakup, sprays, wave mechanism

INTRODUCTION

The presence of undersize and oversize droplets in a kraft recovery boiler contributes to reduced capacity and decreased stability. Experimental studies of black liquor sprays have been performed using a variety of commercial and laboratory scale nozzles operating over a wide range of conditions, and a distribution of droplet sizes was observed in every case.[1,2] In fact, the production of a broad distribution of droplet sizes is a characteristic typical of almost all industrial atomizers.

In order to understand the black liquor spraying process, the fundamental hydrodynamic mechanisms by which the bulk fluid is converted to droplets must be examined. We begin with a description of the various black liquor nozzles and the processes by which they form a fluid sheet. The literature describing how the wave and perforation mechanisms of sheet breakup lead to the formation of cylindrical strands of fluid will then be reviewed. The formation of droplets from liquid strands is usually described using jet breakup theory. These theories will be reviewed with a focus on the conditions expected to dominate in black liquor sprays. Finally, the results of the sheet and jet breakup analyses will be combined to predict droplet sizes.

BLACK LIQUOR SPRAY NOZZLES

Splash Plate Nozzles

A Babcock and Wilcox splash plate nozzle is shown in Figure 1. In this nozzle, the fluid is accelerated through a short entrance length tube and exits from a circular orifice usually one to three centimeters in diameter. The resulting free jet travels a short distance before striking a flat plate at an oblique angle. The forces developed in the region of impact drive the fluid out radially, parallel to the plate surface.[3] The cup region at the rear of the nozzle redirects the backward flowing portion of the fluid toward the front of the splash plate. The resulting fluid sheet has three distinct regions, as is shown in Figure 2.

The edges of the sheet are thick rims formed as a result of the surface tension driven contraction of the fluid in this region. As these rims break up from the action of surface tension, inertial and aerodynamic forces, new rims are rapidly formed.[4] It may be possible to describe rim disintegration and predict the resulting droplet sizes using conventional jet breakup theories.

The redirected back flow impinges the forward-flowing liquid near the center line of the sheet. The complex interactions of the sheet and the impinging recirculation flow would be difficult to characterize analytically; therefore, a description of the breakup of the center of the sheet will rely almost exclusively on experimental observations.

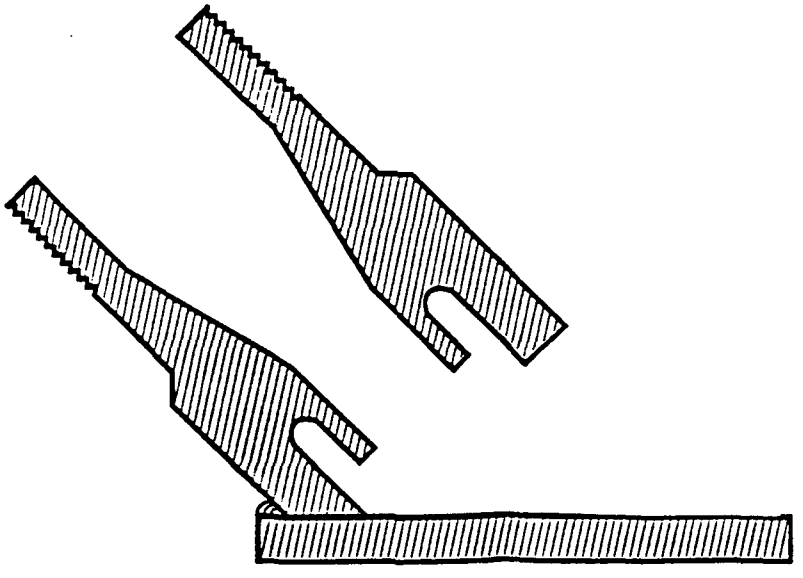

Figure 1: A Babcock and Wilcox splash plate nozzle.

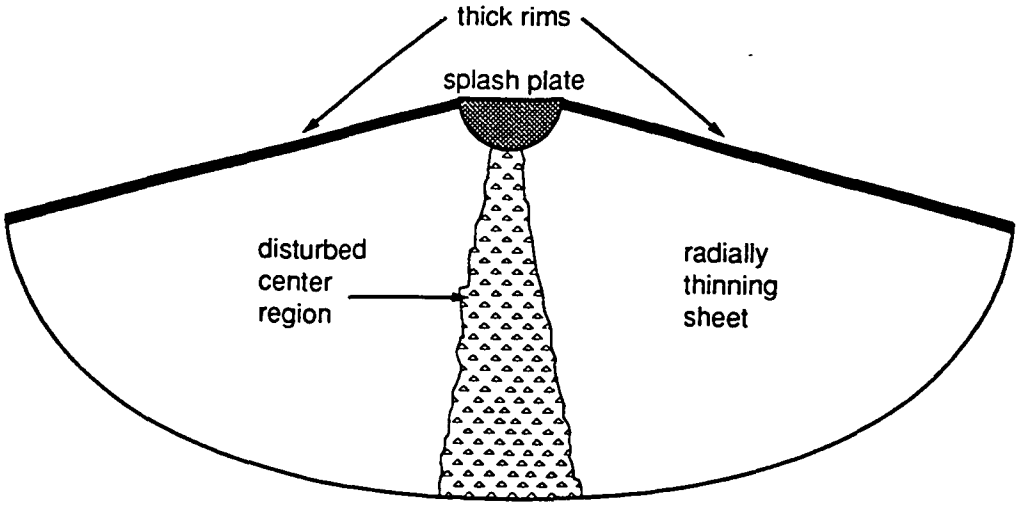

Figure 2: The three regions of a splash plate sheet.

A radially expanding, thinning sheet constitutes the bulk of the spray. For the simple case in which an inviscid circular jet impinges on a plate at a 90° angle, the half thickness of the sheet, h_x, at any radial position, x, measured from the point of jet impact can be obtained from a mass balance.

$$h_x = [D_o^2/16](1/x) \quad (1)$$

An estimate of the half thickness of the undisturbed sheet region of the spray produced by a Babcock & Wilcox splash plate nozzle is given by Equation 2, where α, the angle through which the sheet spreads, is approximately π.

$$h_x = [(U_o/U_s)\cdot(\pi D_o^2/8\alpha)](1/x) \quad (2)$$

In Equation 2, the ratio of jet velocity to sheet velocity (U_o/U_s) is included to account for the decrease in fluid velocity and corresponding increase in sheet thickness that occur as a result of viscous drag on the plate. In most circumstances, the sheet velocity cannot be measured directly, nor can it be predicted exactly unless the impact angle is 90°.[3] However, Obuskovic and Adams[5] developed an expression, based on the principles of conservation of mass and momentum, which can be used to approximate the velocity of a sheet leaving the tip of a splash plate nozzle. The resulting expression, given as Equation 3, correlated well with measurements made near the tip of a B&W nozzle spraying corn syrup/water solutions and black liquor.

$$U_s = U_o\{1 + (64/Re_j)[(x_t/D_o)^3 - (x_v/D_o)^3]\}^{-1} \quad (3)$$

In this expression, x_t is the radial position of the edge of the plate as measured downstream from the point of jet impact. The radial position at which viscous forces are assumed to begin, x_v, is expected to be on the order of the jet diameter, D_o. Using Equation 3, the half thickness of the sheet in the bulk portion of the splash plate spray can be estimated.

$$h_x = [\{1 + (64/Re_j)((x_t/D_o)^3 - (x_v/D_o)^3)\}(D_o^2/16)](1/x) \quad (4)$$

Swirl Cone Nozzles

A sketch of a swirl cone nozzle is shown in Figure 3. As the liquid enters the nozzle, the flow is split in two by the swirl plate. Each half is accelerated along a short curved path, thus increasing the average linear velocity of the fluid and introducing an angular velocity component. The fluid leaves these entrance regions and strikes a curved surface. Here, the liquid spreads out as it exits the orifice of the nozzle, forming a conical, radially expanding sheet.

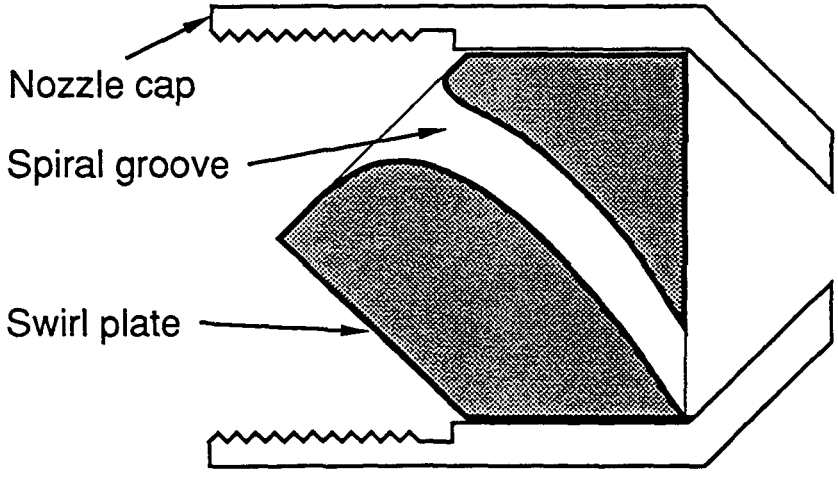

Figure 3: A swirl cone nozzle.

The half thickness of the sheet as a function of the radial distance from the nozzle and the cone angle, β, can be estimated from a mass balance.

$$h_x = [(m_o/4\pi\rho_l U_s)/\tan\beta](1/x) \quad (5)$$

The local cone angle is fixed by a balance of inertial and surface tension forces. Since the magnitudes of these forces vary with the distance from the orifice, the cone angle will also be a function of the position downstream. Taylor[6] developed a prediction for the shape of water bells produced by impinging a jet on a conical diffuser. Using the equation developed for the case of no pressure difference between the inside and outside of the cone and

negligible gravity effects, an expression for tanβ as a function of the downstream distance and the initial cone angle, β_o, can be derived. The result is given as Equation 6. If an initial cone angle of 45° or 60° is assumed, the expression reduces to Equations 7 and 8, respectively.

$$\tan\beta = (1/x)\{1 - \cos(\beta_o)\cosh[\cosh^{-1}(\sec(\beta_o)) - x\sec(\beta_o)]\} \quad (6)$$

$$\tan\beta \approx (1/x)\{1 - 1/\sqrt{2}\cosh[0.8814 - \sqrt{2}x]\}; \quad \beta_o = 45° \quad (7)$$

$$\tan\beta \approx (1/x)\{1 - 1/2\cosh[1.317 - 2x]\}; \quad \beta_o = 60° \quad (8)$$

The breakup of the swirl cone sheet is expected to be similar to that of the bulk sheet portion of the splash plate spray. However, the curvature of the sheet may affect breakup and will be considered.

Fan Spray Nozzles

V-jet and U-jet nozzles are typical of the fan spray style, consisting of a smooth entrance pipe with a spherical cap. The orifice is formed by cutting a groove across the top of this cap. The nozzle discharge coefficient and the spray characteristics are functions of the shape of the groove. While a vast array of groove configurations exists,[7] two common cross sections used in black liquor spraying applications are "V" and "U" shaped. These two groove styles are shown in Figure 4.

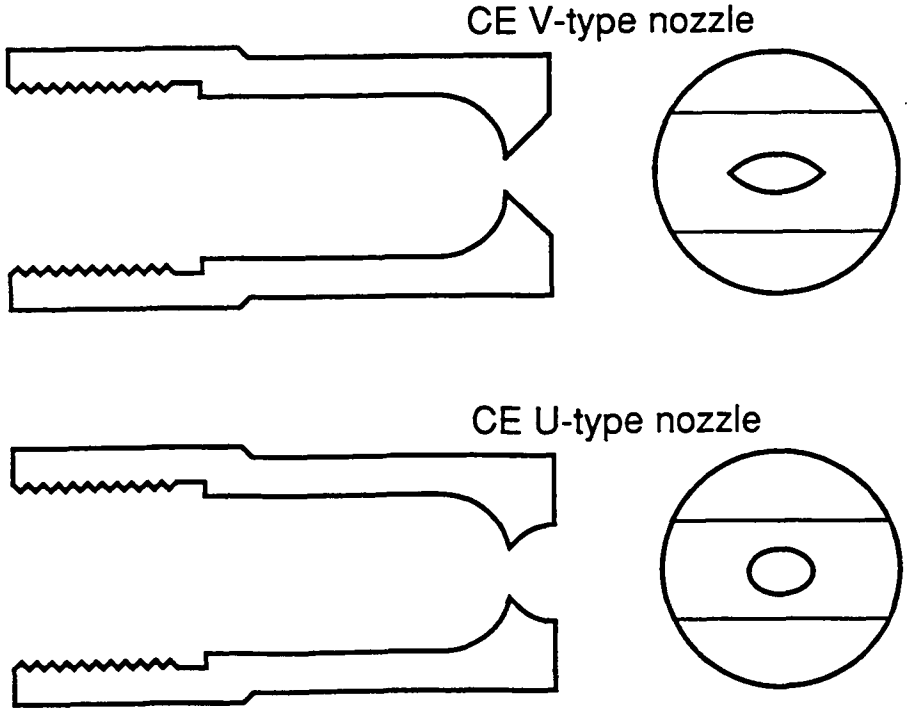

Figure 4: Fan spray nozzles.

The fluid exits the fan spray nozzle as a thick sheet. While the angle through which this sheet spreads varies with nozzle design, it is typically much less than the spread angle for a B&W splash plate nozzle. The resulting sheet thickness is generally much greater than that formed by a splash plate or a swirl cone nozzle.

The actual sheet thickness at a given distance from the nozzle will depend on the nozzle geometry and the initial angular distribution of mass at the orifice. If a uniform sheet thickness is assumed to exist at the point of discharge, Equation 9 can be used to estimate the half thickness of the sheet as a function of the distance downstream.

$$h_x = [A_o/2\alpha](1/x) \qquad (9)$$

MECHANISMS OF SHEET DISINTEGRATION

The Wave Mechanism

Once a sheet of fluid is formed, the surface position will fluctuate as a result of random disturbances in the liquid sheet and the surrounding air. Additionally, a planar liquid sheet moving relative to a second fluid is susceptible to Kelvin-Helmhotz wave instabilities resulting from viscous shear forces.[8] Regardless of the cause, when the position of the air/liquid interface is perturbed locally, aerodynamic, inertial and surface tension forces will be present, and the stability of the boundary will be determined by the balance among them.

The wave mechanism of sheet breakup results from the temporal or spatial growth of disturbances in the position of the boundary. At some critical amplitude, the sheet will break at half wavelength intervals and form bands of fluid. Surface tension forces rapidly contract this fluid into cylindrical strands which ultimately break up into droplets.[9]

A Description of the Relevant Forces

An unperturbed fluid sheet is shown in Figure 5a. In Figure 5b, the sheet surface is perturbed from its planar configuration at points "1" and "2." Once initiated, the disturbances will continue to grow unless other forces in the system overcome the inertia of the fluid.

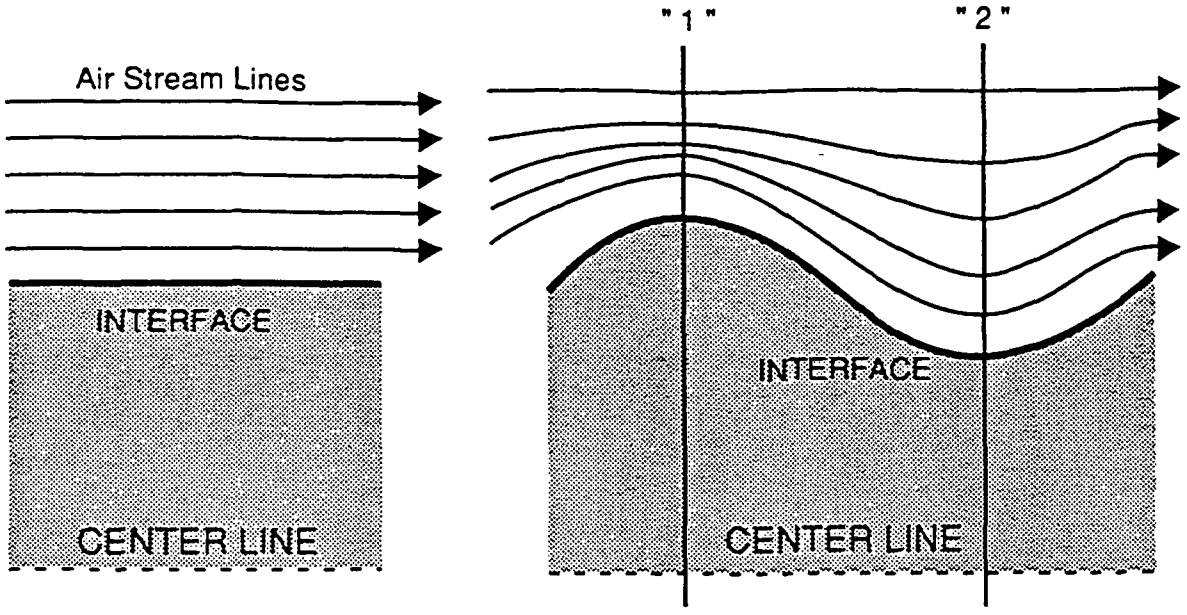

Figure 5: Unperturbed and perturbed liquid sheets.

At points "1" and "2," the perturbations cause an increase in interfacial area, δA. The force required to create this additional area, F_{surf}, is given by Equation 10. If the perturbation is to grow, additional energy would be required to continue increasing the surface area. Thus, surface tension is a stabilizing force which retards the growth of disturbances.

$$F_{surf} = \sigma \delta A \tag{10}$$

In contrast, aerodynamic forces act to increase the magnitudes of the disturbances. At point "1," the air moving relative to the liquid surface will be accelerated as is indicated by the decreased spacing between stream lines. Since the velocity is higher, the gas phase pressure at that point will be lower according to Bernoulli's Equation given below. Similarly, at point "2" the air velocity will be lower and thus the pressure will be higher. The result is a destabilizing pressure gradient which enhances the growth of the disturbances.

$$P/\rho_g + 1/2V^2 = \text{constant} \tag{11}$$

A disturbance in the position of the sheet surface will produce velocity gradients in the fluid. Viscous forces in the fluid sheet will act to inhibit this and thus retard disturbance growth. Therefore, like the surface tension force, viscous forces are expected to stabilize a planar sheet.

Based upon these considerations, it can be inferred that parameters affecting sheet stability might include: the gas and liquid phase densities, the liquid phase viscosity, the interfacial surface tension, and the relative velocity between the phases.

Planar Inviscid Sheets

Numerous analytical studies on the growth of disturbances in fluid sheets have been performed using the ideal flow assumption (inviscid, incompressible, irrotational flow).[10-12] In these studies, the stability of planar fluid sheets was modeled in Cartesian coordinates using a first-order perturbation scheme. A discussion of the important results obtained from these analyses are presented below. The details of first-order perturbation techniques as applied to sheet stability are presented in the Appendix.

A semi-infinite liquid sheet of thickness $2h_o$ travels at a velocity U_s relative to the surrounding air. The positions of the upper and lower surfaces are perturbed from their equilibrium positions, $+h_o$ and $-h_o$, respectively, as shown in Equations 12 and 13. In a perturbation analysis, H is assumed to be much less than one and terms of order H^2 and higher are neglected to obtain a solution valid to first order in the perturbation parameter. In Equation 13, ξ is the phase angle between the disturbances to the upper and lower surfaces.

$$h_+ = +h_o + He^{i(kx-st)} \tag{12}$$

$$h_- = -h_o + He^{i(kx-st+\xi)} \tag{13}$$

In these expressions, the nature of the radial perturbation wave number, k, governs the spatial behavior of the disturbance, while s, the growth rate parameter, governs the temporal behavior. If k is real only, the disturbance will oscillate sinusoidally with position downstream. If k has a positive (negative) imaginary component, the magnitude of the disturbance will decay (grow) exponentially with position downstream. A disturbance which grows exponentially is said to be unstable in an absolute sense.

Similarly for s, a real value indicates an oscillatory disturbance in time, while an imaginary component indicates exponential growth or decay. Because of the negative sign in front of the temporal exponent, the imaginary part of s must be positive for absolute temporal instability to occur.

Expressions for the wave number and the growth rate parameter as functions of the fluid physical properties and the operating conditions are obtained by simultaneously solving the gas and liquid phase continuity equations. The boundary conditions applied are: (a) The normal components of the liquid and gas velocities must vanish at the upper and lower interfaces; (b) the upper and lower gas phase velocities must remain finite as z approaches $+\infty$ and $-\infty$, respectively; and (c) the pressure on the liquid side of the boundary must equal the sum of the gas phase pressure at the interface and the Laplace contribution resulting from the presence of a curved interface. The gas pressure at the interface is obtained from the unsteady Bernoulli equation, and the magnitude of the Laplace contribution is given by the Young-Laplace equation.[13] These equations are included in the Appendix.

Using the procedure outlined above, Hagerty and Shea[10] demonstrated that only two wave forms could exist in the sheet. These are: antisymmetric (sinuous) waves for which the disturbances in the positions of the upper and lower surfaces are in phase ($\zeta=0$), and symmetric (dilational or varicose) waves for which the disturbances are 180° out of phase ($\zeta=\pi$). These wave forms are shown in Figure 6. At all conditions where these disturbances were temporally unstable, the calculated growth rate of the antisymmetric wave was greater than that of the corresponding symmetric wave.[10,11] This theoretical result has been supported by experimental observations.[10,14]

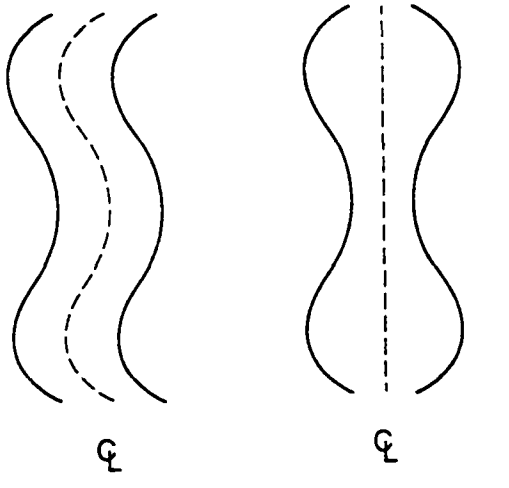

(a) sinuous waves (b) dilational waves

Figure 6: Sinuous and dilational wave forms.

For the case of antisymmetric waves, the temporal growth rate of a disturbance is given by:

$$s = kU_s\tanh(kh_o)/2[\tanh(kh_o)+\gamma]\pm\{4U_s^2k^2\tanh^2(kh_o)-4(\tanh(kh_o)+\gamma)(k^2U_s^2\tanh(kh_o)-\sigma k^3\rho_l)/2[\tanh(kh_o)+\gamma]\}^{1/2} \quad (14)$$

In general, $\gamma \equiv \rho_g/\rho_l << \tanh(kh_o)$, and the expression for the growth rate parameter reduces to:

$$s = kU_s \pm \{[\sigma k^3/\rho_l - \gamma k^2 U_s^2]/\tanh(kh_o)\}^{1/2} \quad (15)$$

In Equations 14 and 15, s can be expressed as the sum of a real and an imaginary part.

$$s = s_r + is_i \quad (16)$$

For a disturbance to be unstable, the imaginary component must exist. Therefore, the term in the square brackets in Equation 15 must be negative. This condition is met when:

$$k < \rho_g U_s^2/\sigma \quad (17)$$

This result was presented by both Hagerty and Shea[10] and Fraser *et al.*[12] as the minimum or critical wavelength of instability. This wavelength, λ_c, is given by Equation 18.

$$\lambda_c = 2\pi\sigma/\rho_g U_o^2 \quad (18)$$

where:

$$k \equiv 2\pi/\lambda \quad (19)$$

The wavelength of the disturbance of maximum growth was predicted by Squire[11] and Fraser *et al.*[12] and is given by Equation 20.

$$\lambda_{opt} = 4\pi\sigma/\rho_g U_s^2 \quad (20)$$

Because first-order perturbation methods were used to obtain these results, the expressions are valid only when the magnitude of the disturbance is small compared to the sheet thickness. However, it is generally assumed that the optimally growing wave at this condition will also dominate at breakup when the amplitude is large.[15]

Planar Viscous Sheets

The results obtained for inviscid planar sheets have been extended by Dombrowski and Johns[9] to include the effects of a finite liquid phase viscosity and a decreasing sheet thickness. They found that for an inviscid sheet, the wave of maximum growth was not affected by sheet thickness and could be calculated using Equation 20.

In a viscous sheet, the growth rate of a disturbance was predicted to be a function of both wavelength and sheet thickness. Thus, the wave with the maximum growth rate at one distance from the nozzle may not be the optimally growing wave farther from the nozzle where the sheet is thinner. However, the results of this analysis

were used to demonstrate the existence of a wave of maximum amplitude at all positions downstream.[9] Therefore, the breakup of the sheet is expected to be dominated by a disturbance of a particular wavelength.

Dombrowski and Johns[9] also found that, as expected, viscous forces retard the growth of perturbations. Therefore, the growth rate of a disturbance in a viscous sheet is less than the growth rate for the corresponding disturbance in an inviscid sheet.

Radially Expanding Viscous Sheets

The liquid sheets formed by typical black liquor spray nozzles expand radially from the nozzle orifice. The resulting cylindrical geometry of the sheet leads to the prediction of waves that are spatially unstable in addition to the temporally unstable waves discussed above.

Weihs[16] performed a theoretical analysis on the stability of a viscous, radially thinning liquid sheet. He found that the temporal instability limit was identical to that calculated by Fraser *et al.*[12] and Hagerty and Shea,[10] and that the wave of maximum growth was a function of sheet velocity and thickness. The magnitude of the change in the wavelength of maximum growth per unit change in sheet thickness was predicted to increase with increasing fluid viscosity.

In addition to temporal instability, Weihs[16] reported a form of spatial instability resulting from the presence of a sinusoidally varying disturbance with increasing successive maxima. This instability could occur even when the sheet was temporally stable.

Curved Sheets

Unlike the planar splash plate sheet, the fluid sheet formed by a swirl cone nozzle is curved. Crapper, Dombrowski and Pyott[17] investigated the effects of this geometry by performing a first-order perturbation analysis on the growth rate of wave disturbances in an annular fluid film. The results of this analysis can be extended qualitatively to the case of a swirl cone spray in which the radius of the annulus increases with distance from the nozzle.

Crapper *et al.*[17] predicted both the growth rate of disturbances and the wave of maximum growth to be functions of the inner radius of the annular film. However, the effect was negligible when the inner radius of the annular spray was greater than about one centimeter. In general, the inner radius of a typical black liquor swirl cone spray is much greater than this critical value. Thus it appears that the curvature of the swirl cone sheet can be neglected when analyzing its stability.

Several features of wave breakup can be inferred from the theories discussed. First, while the source of the wave disturbances is unknown, it is reasonable to assume that, if they result from random fluctuations in the sheet and the surrounding air, then all wavelengths are equally likely to occur and all initial amplitudes will be of the same order of magnitude.[9] Second, all disturbances for which the imaginary part of the temporal growth rate parameter (s_i) is positive will grow exponentially, without bound. Furthermore, a disturbance of a particular wavelength will dominate in the region of breakup. When the amplitude of this wave reaches a critical value, the liquid will break into ribbons which will collapse into cylindrical strands and ultimately form droplets. Since a single wave is predicted to cause the formation of strands from the sheet, all strands so produced will have the same diameter. As will be shown in a later section, this leads to the prediction of droplets of a single size.

The Perforation Mechanism

A second mechanism of sheet breakup is the initiation and growth of perforations. Once formed, a hole in a fluid sheet is rapidly expanded by surface tension forces and the fluid is drawn up into a thick rim about the hole.[7] The expansion of a perforation is halted when this rim reaches the edge of the sheet or another perforation rim. The result is a web of interconnected strands of fluid which will break up under surface tension and aerodynamic forces to form droplets.

Sources of Perforations

Fraser *et al.*[12] reported evidence of perforation breakup in water sheets formed in a subatmospheric environment. They suggested that the perforation mechanism only became dominant when aerodynamic forces were suppressed and the sheet was stable to wave disturbances.

Clark and Dombrowski[4] reported observing sheet breakup by the perforation mechanism when spraying water into high temperature environments. Below 300°C, the wave mechanism dominated, while above 300°C both the wave and perforation mechanism were observed. The importance of the perforation mechanism relative to the wave mechanism increased with ambient temperature. The perforations were reportedly caused by an interaction between the aerodynamic waves discussed previously and electrohydrodynamic waves resulting from the accumulation of negative charges on the sheet surface due to the ionized gases in the high temperature environment.[4]

In both of these studies, care was taken to eliminate flow disturbances upstream of and in the nozzle. Dombrowksi and Fraser[7] showed that the presence of turbulence in the nozzle can lead to localized disruptions of the sheet. These can then lead to holes, and breakdown occurs via the perforation mechanism. Dombrowski and Fraser were studying the performance of fan spray nozzles and found that a perforated sheet was formed at nozzle Reynolds numbers above 20,000 to 40,000, depending on the sheet velocity. Below this range, unperforated sheets were observed.

Dombrowski and Fraser[7] showed that unwetted particles would cause perforations if the particle size was on the order of the sheet thickness. The presence of particles wetted by the test fluid did not, however, result in perforations, regardless of their size.

Clark and Dombrowski[4] demonstrated that the release of dissolved gases was <u>not</u> responsible for the formation of perforations. They detected no difference between the breakup of sheets of water supersaturated with air and the breakup of sheets of distilled water in which the air content was reduced to 1 ppm.

<u>Growth Rate of Perforations</u>

The growth rate of a perforation is rapid, provided its initial diameter is larger than the thickness of the sheet. Perforations smaller than this will close back into the sheet.[18] Fraser *et al.*[12] derived an expression for the velocity of the rim of a perforation growing in a planar liquid sheet. This analysis was based on the balance between the surface tension force driving the expansion and the increase in inertia of the growing rim. The resulting equation is given below.

$$e = (\sigma/h\rho_l)^{1/2} \quad (21)$$

If the sheet is expanding radially, the half thickness will be proportional to the reciprocal of the distance from the nozzle as was shown in Equations 2, 4, 5, and 9. In each case, a general proportionality constant, k_o, can be used to replace the term in square brackets, reducing these expressions to Equation 22. In the case of Equation 4, k_o is not a true constant as tanβ varies with downstream position.

$$h_x = k_o/x \quad (22)$$

For a perforation of radius r_p, centered at distance R_o from the nozzle, the distance from the orifice to a point on the rim is given by Equation 23.

$$x = [R_o^2 + r_p^2 - 2R_o \cdot r_p \cdot \cos(\theta)]^{1/2} \quad (23)$$

In some cases, the distance from the nozzle to a point on the rim can be approximated by the distance to the center of the perforation (zeroth order in r_p). When the radius of the perforation is of the same order as the distance from the nozzle, a first-order correction in r_p must be applied. The resulting expressions are given as Equations 24 and 25, respectively.

$$x_0 = R_o \quad (24)$$

$$x_1 = R_o - r_p\cos(\theta) \quad (25)$$

Fraser *et al.*[12] used the zeroth-order approximation to estimate the growth rate of a perforation in a thinning sheet. Their result is given as Equation 26. In this work, the effects of applying the first-order approximation are demonstrated. This expression for rim velocity is given as Equation 27.

$$e_0 = \mathrm{sqrt}(2\sigma/k_o\rho_l)R_o^{1/2} \quad (26)$$

$$e_1 = \mathrm{sqrt}(2\sigma/k_o\rho_l) \cdot [R_o - 0.8 \cdot r_p\cos(\theta)]^{1/2} \quad (27)$$

The zeroth-order equation predicts a uniformly expanding perforation, while the first-order solution predicts that the perforation will grow faster in the downstream direction ($\theta=\pi$) where the sheet is thinner, and slower in the upstream direction ($\theta=0, 2\pi$) where the sheet is thicker. The magnitude of this variation is a function of the ratio of the perforation radius to the distance from the nozzle as is shown in Figure 7.

The radius of a strand formed via the perforation mechanism will depend on a number of parameters, including location downstream at which it was formed, time for growth, and interactions with other strands. Therefore, unlike the wave mechanism, a wide range of strand sizes is expected to form. As will be shown in the

following section, this appears to be a prerequisite for the formation of the wide distribution of droplet sizes observed in spray experiments.

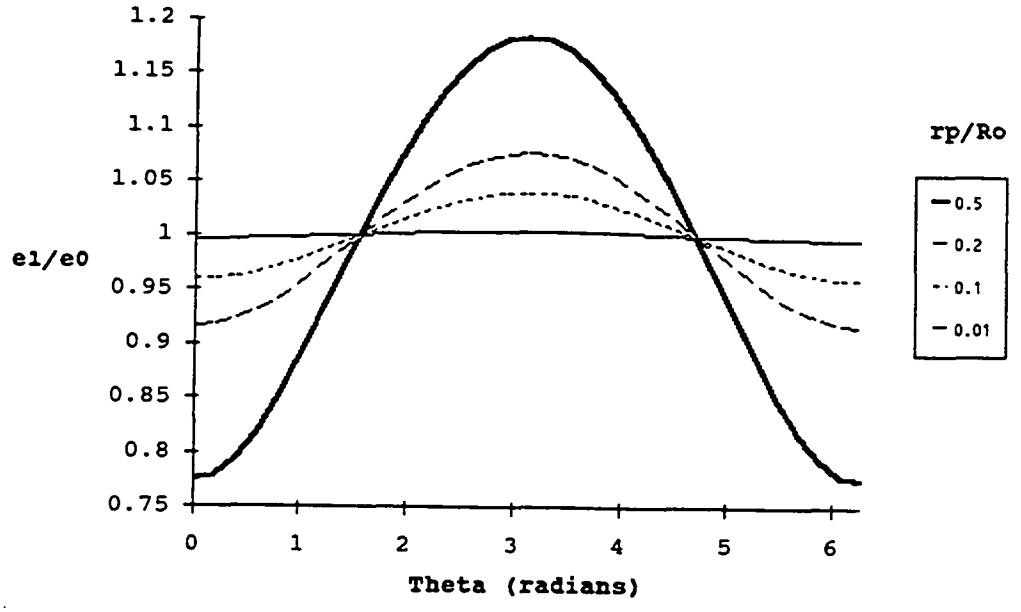

Figure 7: Velocity variation vs. theta as a function of r_p/R_o.

THEORIES OF STRAND BREAKUP

Both the wave and perforation mechanisms lead to the formation of cylindrical strands of liquid. The formation of droplets from these strands has often been treated using jet breakup theories. Both experimental and theoretical studies of the stability of fluid jets have been reported in the literature.[19-25]

Rayleigh's Analysis

One of the first theoretical treatments of the stability of capillary jets was performed by Lord Rayleigh.[19] In his analysis, Rayleigh examined the stability of a stationary, infinitely long, inviscid jet with a circular cross section. In addition to these approximations, the interactions of the liquid with the surrounding air were neglected. This idealized jet was then subjected to a small radial perturbation of the form shown in Equation 28.

$$r = r_o + a_n \cdot \exp(st) \cdot \cos(n\theta) \cdot \cos(kz) \qquad (28)$$

In this expression the axial wave number, k, can take on any positive value, while the tangential wave number, n, is restricted to positive integer values.

Rayleigh[19] showed that a liquid cylinder subject to such a disturbance would be stable to all perturbations for which n>0 and thus, only axisymmetric disturbances (n=0) were examined. The result of Rayleigh's analysis is the classic equation relating the growth rate, s, and the dimensionless wave number, $k \cdot r_o$, of a disturbance.

$$s^2 = (\sigma/\rho_l \cdot r_o^3) \cdot [I_1(kr_o)/I_0(kr_o)] \cdot [kr_o - (kr_o)^3] \quad (29)$$

In Equation 29, the growth rate parameter can be made dimensionless with respect to $(\sigma/\rho_l \cdot r_o^3)^{1/2}$. The dimensionless growth rate parameter is defined as ψ and the dimensionless wave number, $k \cdot r_o$, is redefined as ξ. Equation 29 then becomes:

$$\psi^2 = [I_1(\xi)/I_0(\xi)] \cdot [\xi - \xi^3] \quad (30)$$

Since ξ must be greater than zero, and since $I_0(\xi)$ and $I_1(\xi)$ are always real and greater than or equal to zero when ξ is greater than zero, it can be shown that the condition for instability ($\psi^2 > 0$) is met only when $\xi < 1$. This occurs when the wavelength of the disturbance is greater than the circumference of the undisturbed jet. It should also be noted that a wavelength of maximum growth rate exists. This behavior is more clearly seen in the plot of growth rate versus wave number shown in Figure 8.

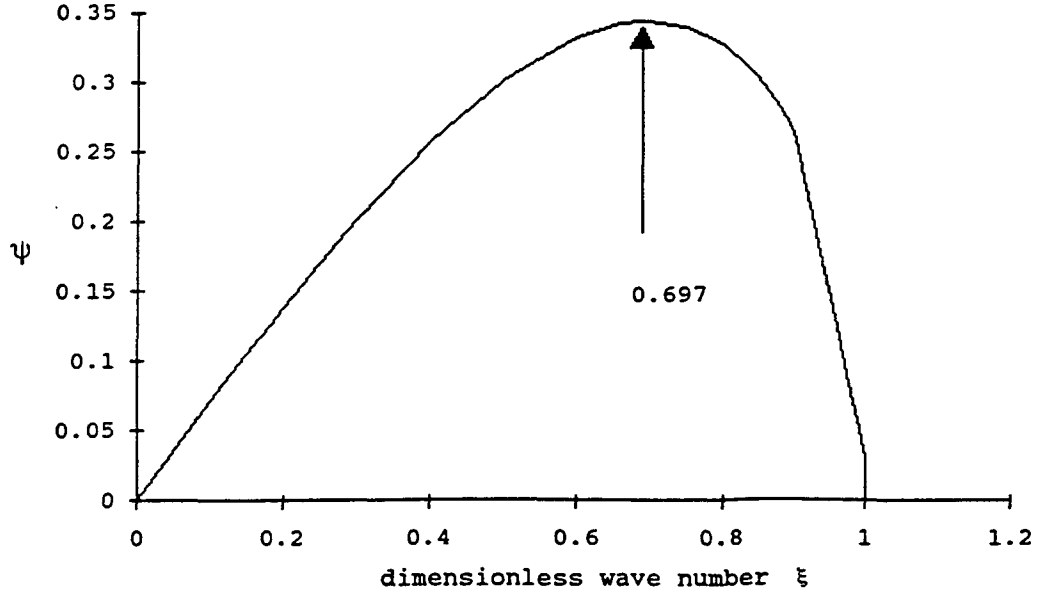

Figure 8: Dimensionless growth rate parameter as a function of the dimensionless wave number based on Rayleigh's solution.

The dimensionless wave number of maximum growth is independent of the fluid physical properties. From this it can be inferred that for all strands to which Equation 30 applies, the dimensionless wave number of maximal growth is a constant (ξ=0.697). Thus, if a single droplet is assumed to form from each wavelength of the disturbance, then all such strands should break up into uniformly sized drops. Furthermore, if a sheet produces uniform sized strands under conditions at which Rayleigh's analysis can be applied, then the entire spray would be composed of droplets of a single size. In practice, a wide distribution of droplet sizes is produced.[1]

Viscous and Aerodynamic Forces

Weber[20] incorporated liquid viscosity and liquid/air interactions into a theory of jet breakup. His analysis resulted in a quadratic equation for growth rate as a function of dimensionless wave number. This equation can be made dimensionless using the same definitions as were applied to Rayleigh's solution. In Equation 31, the Weber and Reynolds numbers are based on the liquid properties.

$$\psi^2 + \psi(3 \cdot We_r^{1/2}/Re_r)\xi^2 = 1/2(1-\xi^2)\xi^2 + 1/2(We_\rho)(\rho_g/\rho_l)\xi^3 [K_0(\xi)/K_1(\xi)] \quad (31)$$

The addition of viscous and aerodynamic forces has modified the growth rate expression; however, a wavelength of maximal growth is still predicted. Therefore, a single droplet size is expected to be produced from a strand of a given diameter.

Nonlinear Analyses

Both Rayleigh's[19] and Weber's[20] analyses are based on linear perturbation theory and their results are valid only when the amplitude of the radial disturbance is small compared to the strand diameter. Nonlinear terms will become important as the disturbance grows to the point of breakup. Nonlinear capillary instability has been studied by numerous researchers[21-24] and the results of one of these studies will be discussed here.

Lafrance[21] performed a third-order perturbation analysis on an inviscid, circular jet. This analysis did not include aerodynamic interactions. The two key results were: (1) The third-order solution still predicts an optimally growing disturbance, and (2) at certain conditions, the existence of a smaller satellite drop is predicted in addition to the main drop. Thus, nonlinear theory predicts the formation of a small number of discrete droplet sizes for a given strand diameter.

Velocity Profiles Around a Strand

The literature on strand breakup deals almost exclusively with a jet travelling parallel to its axis. Yet, from reviewing images of sprays, it is expected that a significant percentage of the strands produced in black liquor spraying processes will have the dominant component of velocity perpendicular to the axis. This cross flow of air is expected to interact with the liquid jet differently than would a coaxial flow.

Weihs and Frankel[25] performed a theoretical analysis on an initially circular fluid cylinder in a cross flowing air stream. The equilibrium cross section of the strand was calculated as a second-order perturbation using the Weber number as the perturbation parameter. The analysis was stated to be valid up to a Weber number of approximately 0.5.

The resulting cross section was subjected to a radial disturbance similar to that assumed by both Rayleigh[19] and Weber[20]. The form of this disturbance is given by Equations 32 and 33.

$$r = r_o(\theta)\cdot(1 + \eta) \tag{32}$$

$$\eta = \eta_o\{B_o + \Sigma[A_n\cdot\sin(n\theta) + B_n\cdot\cos(n\theta)]\}\cdot\exp(st+ikz) \tag{33}$$

In their solution for growth rate versus wave number, Weihs and Frankel[25] showed that a perturbation with a tangential wave number of n would be unstable only if $We \geq (1/2)(n+1)$. Since the results of this analysis are restricted to conditions when $We \leq 0.5$, only axisymmetric disturbances (n=0) were considered in the stability analysis.

Weihs and Frankel[25] solved for the growth rate of an axisymmetric disturbance as a function of the dimensionless axial wave number, ξ. As with the previous studies, a wavelength of maximum growth was predicted. This wavelength increases with decreasing Weber number. Although incorporating the effects of a cross flow of air has modified the growth rate expression, a single droplet size is still predicted.

The main conclusion to be drawn from these analyses is that a strand is expected to break up into a discrete number of droplet sizes. Therefore, to account for the broad distribution of droplet sizes produced in industrial spraying applications, a distribution of strand sizes must be produced.

EXPERIMENTAL OBSERVATIONS

A variety of experimental studies on spray behavior has been performed by the Institute of Paper Science and Technology in the last four years. Flash x-ray images of black liquor sprays produced by splash plate and swirl cone nozzles were collected and drop size distributions were obtained.[1] Pressure drop/flow rate data were collected for B&W splash plate, and U- and V-jet nozzles.[26] Velocity/sheet thickness relationships were obtained for the B&W splash plate nozzle.[5] High-speed video images of model fluid and black liquor sprays have been collected using a variety of conventional and model nozzles. High-speed video images of swirl cone, splash plate and V-jet black liquor sprays were obtained through the gun port of an operating recovery boiler. These experiments have provided a unique opportunity to observe various stages of the breakup process.

Predominance of the Perforation Mechanism

Perhaps the most important observation thus far has been the evidence that swirl cone and splash plate sheets appear to break up almost exclusively via the perforation mechanism. This mechanism dominated at all operating conditions including both low-viscosity water sprays (1 cp) and high-viscosity black liquor and corn syrup/water sprays (50-300 cp). It was observed when spraying into a room temperature environment and also when spraying into the high temperature recovery boiler environment. The source of the perforations has not yet been determined.

While unwetted suspended solids may contribute to the formation of perforations in black liquor sprays, they would not be expected to cause the perforations observed in water, corn syrup/water and glycerol/water sprays. The electrohydrodynamic mechanism may be a contributing factor in the recovery boiler; however, it cannot be responsible for the perforations in the laboratory spray studies. The presence of turbulence in the nozzle is still being investigated, but the nozzle Reynolds numbers are much lower than the 20,000 to 40,000 reported by Dombrowksi and Fraser.[7] Given the apparent predominance of the perforation mechanism, it is expected that a single mechanism is responsible for the formation of holes at all operating conditions tested.

Model Nozzle Studies

Studies are being performed on simplified splash plate sprays. A jet is formed by a nozzle with a short, straight orifice region 3.8, 4.8, or 6.4 millimeters in diameter. The jet impinges a polished, five-centimeter diameter steel plate at a 90° angle. A circular, radially expanding, thinning sheet is thus formed.

Wave fronts have been observed in the fluid on the plate surface forming concentric rings about the point of jet impact. These waves persist into the full sheet region off the splash plate edge. However, it does not appear that these waves are growing exponentially, nor do they appear to lead to the breakup of the sheet via the wave mechanism. Dombrowski and Fraser[7] described a similar disturbance in the sheet formed by the impingement of two axisymmetrically opposed jets. They attributed these circumferential waves to turbulence in the nozzle. Taylor[27] observed circumferential waves in swirl cone sheets. These were suggested to be symmetric waves resulting in thickness variations in the sheet.

The condition of the surface at the edge of the plate has been shown to have a significant affect on the structure of the resultant sheet. A small discontinuity in the plate edge disrupts the fluid sheet. This disturbance spreads out radially from the plate imperfection and influences a large region of the spray. Both Taylor[28] and Huang[29] reported on this phenomenon. Taylor showed that a small disturbance in a radially expanding sheet would result in a cadioid wave emanating from the point of the plate defect. Huang demonstrated that the shape of the leading edge of a sheet could be defined by a series of cadioid wave fronts and suggested that these waves resulted from disturbances at the nozzle.

Careful polishing of a sharp-edged plate appears to have eliminated these disturbances. Attempts were made to produce a smoother sheet using a plate with a polished, rounded edge. However, a disperse wedge of droplets was formed rather than a sheet as the point of fluid release from the plate was not well defined.

Sheet Characteristics

Images of glycerol/water sprays have been obtained with a Xybion ISG-250 high-speed video camera. Back lighting of the fluid sheet has provided the most detailed pictures obtained thus far. Small wave-like disturbances have been observed in the sheet at all distances from the plate edge out to the point of breakup. These

disturbances appear to cause local thin spots in the sheet surrounded by thick bands. It appears that a large percentage of the observed perforations are initiated in these thin spots. The holes grow rapidly until they encounter the thick bands, thus taking on the shape of the initial disturbance. Further investigation into this phenomenon is ongoing.

The source of the wave disturbances and resulting thin spots has not been established. However, turbulence in the nozzle has been cited as an explanation for point disturbances in fan spray sheets.[7] While steps will be taken to eliminate disruptions in the fluid jet prior to its impact on the splash plate, turbulence generated in the region of jet impact may dominate. Alternatively, the thick and thin regions may be the result of the symmetric waves similar to those observed by Taylor in swirl cone sheets.[27]

Perforation Number Density

A series of tests has been performed using 4.8 mm and 6.4 mm orifice nozzles. Glycerol/water sprays were formed at five jet velocities ranging from 12.5 to 22.5 m/sec. One thousand images were observed at each of seven distances ranging from 8 to 21 cm downstream of the point of jet impact. The number of perforations in the sheet was counted at each combination of orifice diameter, jet velocity and downstream distance.

It was clear from these studies that perforations are not formed at the edge of the plate, but rather occur over a considerable range starting at some finite distance downstream. At all but the highest velocities, no perforations were observed closer than 12 cm from the point of jet impact. Beyond this point, the number of perforations increased with position downstream.

Since experimental observations have established that perforations are formed over a range of downstream positions, it should be possible to predict the formation of a distribution of droplet sizes. A number of assumptions will be made in the following derivation. First, since the observed ratio of perforation radius to distance downstream was less than 0.1, the zeroth-order expression derived by Fraser *et al.*[12] (Equation 26) will be used to estimate perforation growth rates with an expected error of less than five percent. Second, the perforations will be assumed to remain circular as they grow to the point of sheet breakup. Thus, the interaction of neighboring perforations and the resulting increase in strand diameter that occurs when rims merge are neglected. The tangential

stretching of the rim that results from the radial expansion of the sheet is also neglected. Third, despite the expected closed loop shape of the strands, Rayleigh's analysis will be used to calculate droplet diameters based on the predicted rim sizes. Therefore, the formation of satellite drops is neglected. Finally, the clumps of fluid observed to exist between neighboring perforations at breakup will be neglected. These assumptions will result in the prediction of a narrower distribution of droplet sizes than that expected to be observed experimentally.

To avoid confusing notation with previous derivations, the following definitions are applied:

a = radius of a perforation

b = radius of the rim surrounding a perforation

c = radius of a droplet

o = subscript denoting the initial value of a variable

f = subscript denoting the final value of a variable at breakup

N_p new perforations of radius a_o are observed at a distance x_o downstream. The rate of change in perforation radius with position downstream is given as Equation 34.

$$da/dx = (da/dt)(dt/dx) = (e_0)(1/U_s) \tag{34}$$

Using the expression for e_0 obtained by Fraser *et al.*,[12] the growth rate equation becomes:

$$da/dx = (2\sigma/k_o\rho_l U_o^2)^{1/2} x^{1/2} \tag{35}$$

Equation 35 can be integrated to determine the radius of each perforation at the point of breakup, x_f.

$$a_f = [8\sigma/9k_o\rho_l U_o^2]^{1/2}[x_f^{3/2} - x_o^{3/2}] + a_o \tag{36}$$

The total length of one perforation rim is given by:

$$L = 2\pi a_f \tag{37}$$

Therefore, the total length of all strands initiated at position x_o is:

$$L_{tot} = N_p \cdot L \tag{38}$$

The radius of the strand can be determined from a mass balance as all of the mass which was located in a perforation of area πa_f^2 in a sheet of thickness 2h must be collected in a rim of length $2\pi a_f$ and cross-sectional area πb^2.

$$2\pi a_f(\pi b^2) = 2h\pi a_f^2 \tag{39}$$

With h given by k_o/x_f,

$$b = (a_f k_o/\pi x_f)^{1/2} \quad (40)$$

Rayleigh's theory can be used to predict the wavelength of optimum growth in a strand of radius, b.[19]

$$k_{max}b = 0.697$$

$$(2\pi/\lambda_{max})b = 0.697$$

$$\lambda_{max} \approx 9b \quad (41)$$

If a single droplet is assumed to form from each wavelength of the disturbance, the drop radius, c, can be calculated from a mass balance.

$$\pi b^2 \lambda_{max} = 4\pi c^3/3$$

$$c = [27b^3/4]^{1/3} \quad (42)$$

The number of droplets formed from one strand is assumed to equal the length of the strand divided by the wavelength of the disturbance.

$$N_d = L_{tot}/\lambda_{max} \quad (43)$$

Equations 34 through 43 can be used to predict number and volume fraction distributions of droplet sizes formed if the rate of formation of perforations as a function of downstream distance (N_p as a function of x_o) is known. Three sample perforation distributions are shown in Figure 9. The "linear" curve represents a linearly increasing number of new perforations with position downstream. The "exponential" curve represents an exponentially increasing rate of new perforation formation with position downstream. The maximum number of new perforations is formed at some distance near the point of breakup and then falls to zero. This distribution resembles perforation formation rates observed experimentally. However, because of the significant disruption of the sheet near the region of breakup, it is not known if the number of new perforations formed near the breakup point drops to zero immediately. If new perforations form in this region, but at a significantly reduced rate, the perforation rate would resemble the "skewed" distribution. These hypothetical perforation number distributions have been normalized so that the same number of perforations is formed in all cases. The resulting droplet size distributions are shown in Figure 10. In order to calculate the size distributions reported, a set of operating conditions was assumed. These conditions are summarized in Table 1 and are typical of the glycerol/water sprays being investigated at the Institute of Paper Science and Technology.

While the procedure outlined above neglects much of the physics involved in the perforation breakup process, the curves shown in Figure 10 have the characteristic shape of measured droplet size distributions.[1] Thus, it appears that the predominance of the perforation mechanism may account for the wide variation in droplet size observed in black liquor atomization processes. Further refinements of the analytical description of the production of droplets from the web of strands and clumps of fluid formed during perforation breakup must be made. Also, data must be collected on both droplet size and perforation number density distributions for given conditions, and predicted and measured values must be compared.

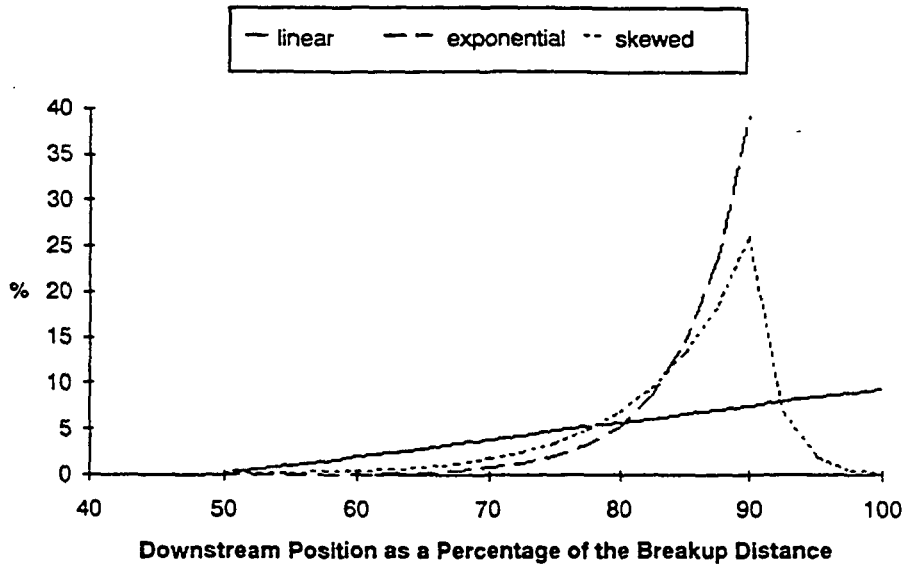

Figure 9: Hypothetical perforation number density distributions.

Table 1: Assumed operating conditions for hypothetical spray system.

surface tension	= 60 dyne/cm
liquid density	= 1200 kg/m^3
sheet velocity	= 15 m/sec
k_o [$h_x = k_o(1/x)$]	= 5 x 10^{-6} m^2
initial perforation radius	= 1 mm

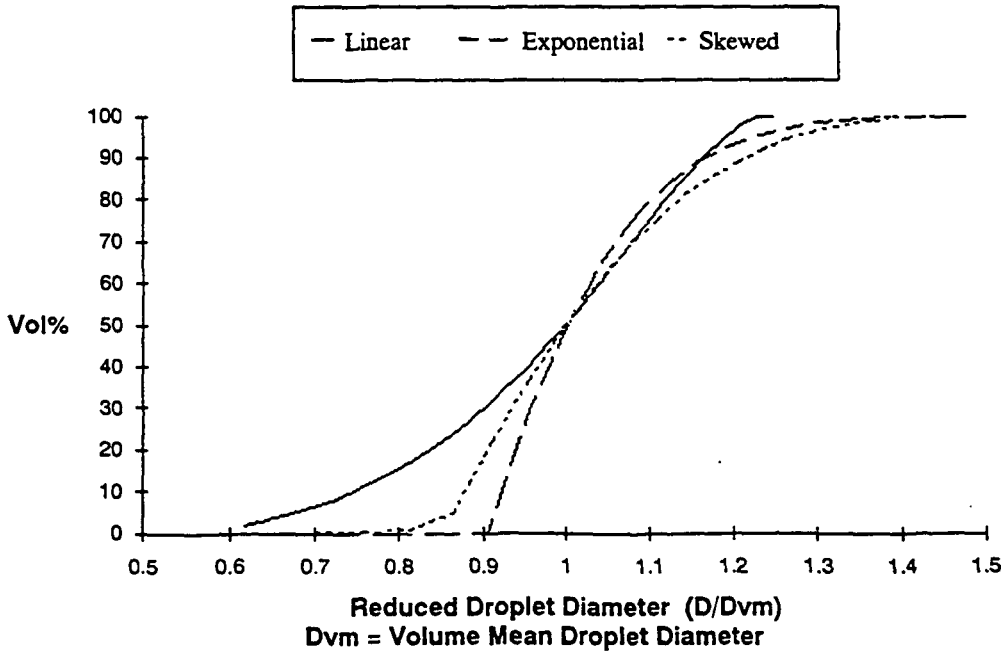

Figure 10: Cumulative volume percent distribution of droplet sizes.

DISCUSSION

Both the wave and the perforation mechanisms of sheet breakup lead to the formation of strands as an intermediate step prior to the production of droplets. However, the existence of strands of uniform size is predicted from the wave mechanism, while the formation of strands with a distribution of sizes is predicted from the perforation mechanism. As only a discrete number of droplet diameters is expected to be formed from strands of a single diameter, this distribution of strand sizes is required to account for the broad distribution of droplet sizes typical of black liquor sprays.

A procedure has been developed to predict the droplet size distribution expected for a given distribution of perforations. Further work is required to determine the effects of various operating parameters on the perforation number density. Ultimately, this information will be combined to predict the droplet size distribution of black liquor sprays and the influence of variations in fluid physical properties and changes in firing conditions.

APPENDIX

First-Order Perturbation Analysis of Sheet Stability

The following derivation follows closely that presented by Hagerty and Shea:[10]

A semi-infinite liquid sheet of thickness $2h_o$ moves with a velocity U_o relative to the gas phase. The positions of the upper and lower interfaces are given by Equations A1 and A2, where H is a perturbation parameter and, as such, is much less than one. In the expression for h_-, ζ is an arbitrary phase angle between the disturbances to the upper and lower surfaces.

$$h_+ = +h_o + He^{i(kx-st)} \tag{A1}$$

$$h_- = -h_o + He^{i(kx-st+\zeta)} \tag{A2}$$

Because the flow is assumed ideal, the components of the gas and liquid velocities can be defined in terms of a velocity potential.

$$\underline{v}_j = -\nabla\varphi_j \tag{A3}$$

where: j = l, liquid phase
j = g, gas phase

The velocity potential in each phase can be written as the sum of the base, unperturbed potential and the perturbed potential. For the liquid phase, the base potential is given by $-U_s x$, representing a uniform flow in the positive x direction. The base flow of the gas phase is assumed to be zero, therefore the base potential is a constant chosen to be zero. Equation A3 can then be expressed as:

$$\varphi_l = -U_s x + \Phi_l(z)e^{i(kx-st)} \tag{A4}$$

$$\varphi_g = \Phi_g(z)e^{i(kx-st)} \tag{A5}$$

The continuity equation can be written as the Laplacian of the velocity potential.

$$\nabla^2\varphi_i = (\partial^2\varphi_i/\partial z^2) + (\partial^2\varphi_i/\partial x^2) = 0 \tag{A6}$$

The velocity potential in the liquid phase ($h+ \geq z \geq h-$) is determined by substituting Equation A4 into Equation A6, keeping terms to first order in the perturbation variables and subtracting the base case solution. The resulting differential equation and the full velocity potential are given below.

$$\partial^2\Phi_l(z)/\partial z^2 - k^2\Phi_l(z) = 0 \tag{A7}$$

$$\varphi_l = -U_s x + [C_1\sinh(kz) + C_2\cosh(kz)]e^{i(kx-st)} \tag{A8}$$

Likewise, expressions can be obtained for the upper and lower gas phase velocity potentials using the boundary condition that v_x and v_z must remain finite as $x \rightarrow \infty$ and $x \rightarrow -\infty$.

$$\varphi_{g,u} = C_3 e^{-kz} e^{i(kx-st)} \quad (x \geq h_+) \tag{A9}$$

$$\varphi_{g,l} = C_4 e^{+kz} e^{i(kx-st)} \quad (x \leq h_-) \tag{A10}$$

The constants, C_1 - C_4, are determined by applying the condition that the velocity of the fluids normal to the boundaries must be zero at the boundaries. All boundary conditions can be applied at the unperturbed interface positions, $\pm h_o$, to first-order accuracy in the perturbation parameter.

$$v_z \big|_{z=h+/-} = Dh/Dt \tag{A11}$$

Where D/Dt is the substantial derivative defined as:

$$D/Dt = \partial/\partial t + v \bullet \nabla \tag{A12}$$

The resulting expressions for the liquid and upper and lower gas phase velocity potentials are given as Equations A13 - A15.

$$\varphi_l = -U_s x + [ih(s/k - U_s)/2][\sinh(kz)(1+e^{i\zeta})/\cosh(kh_o) + \cosh(kz)(1-e^{i\zeta})/\sinh(kh_o)]e^{i(kx-st)} \tag{A13}$$

$$\varphi_{g,u} = [-ish/k]e^{-k(z-h_o)}e^{i(kx-st)} \tag{A14}$$

$$\varphi_{g,l} = [+ish/k]e^{+k(z+h_o)}e^{i(kx-st)} \tag{A15}$$

The final boundary condition is the continuity of pressure across the interfaces.

$$P_l = P_g + \sigma(1/R) \tag{A16}$$

The pressures in the liquid and gas phases can be determined from the unsteady Bernoulli Equation.

$$P_j = K_j + \rho_j\{\partial\varphi_j/\partial t - 1/2[(-\partial\varphi_j/\partial z)^2 + (-\partial\varphi_j/\partial x)^2]\} \tag{A17}$$

Equation A17 must be solved for the gas and liquid phase pressures at both interfaces. The constants, K_j, can be determined by applying the unsteady Bernoulli equation to the unperturbed sheet. Thus:

$$C_g = P_\infty \text{ and} \tag{A18}$$

$$C_l = P_\infty + (1/2)\rho_l U_s^2 \tag{A19}$$

The resulting expressions can be substituted into Equation A16 along with expressions for the radius of curvature at the upper and lower surfaces.

$$(1/R)_u = -(\partial^2 h/\partial x^2) = k^2 H e^{i(kx-st)} \tag{A20}$$

$$(1/R)_l = +(\partial^2 h/\partial x^2) = -k^2 H e^{i(kx-st+\zeta)} \tag{A21}$$

After making the necessary substitutions, Equation A16 becomes at the upper boundary:

$$\sigma k^2 = (k\rho_l/2)(s/k-U_s)^2[\tanh(kh_o)(1+e^{i\zeta}) + \coth(kh_o)(1-e^{i\zeta})] + \rho_g s^2/k \quad (A22)$$

and at the lower boundary:

$$\sigma k^2 e^{i\zeta} = (-k\rho_l/2)(s/k-U_s)^2[-\tanh(kh_o)(1+e^{i\zeta}) + \coth(kh_o)(1-e^{i\zeta})] + (\rho_g s^2/k)e^{i\zeta} \quad (A23)$$

Taking the sum and the difference of Equations A22 and A23 and rearranging leads to:

$$0 = (1+e^{i\zeta})[(k\rho_l)(s/k-U_s)^2\tanh(kh_o) + \rho_g s^2/k - \sigma k^2] \quad (A24)$$

$$0 = (1-e^{i\zeta})[(k\rho_l)(s/k-U_s)^2\coth(kh_o) + \rho_g s^2/k - \sigma k^2] \quad (A25)$$

Only two solutions to this set of equations exist, leading to the restriction that ζ is either 0 or π.

CASE I: $\zeta=0$, sinuous waves

If $\zeta=0$, then $(1-e^{i\zeta})$ is equal to zero, and Equation A25 is satisfied. To satisfy Equation A24, the term in square brackets must be zero. This term can be rearranged to yield a quadratic equation in s, the growth rate factor. When this equation is solved, neglecting the density ratio ρ_g/ρ_l compared to $\tanh(kh_o)$, the following expression for s as a function of the wave number, k, is obtained.

$$s = U_s k \pm[(\sigma k^3/\rho_l - k^2U_s^2\rho_g/\rho_l)/\tanh(kh_o)]^{1/2} \quad (A26)$$

This relation is identical to Equation 15.

CASE II: $\zeta=\pi$, dilational waves

If $\zeta=\pi$, then $(1+e^{i\zeta})$ is equal to zero and Equation A24 is satisfied. Then, to satisfy Equation A25, the term in square brackets is set equal to zero. As with Case I, a quadratic expression in the growth rate parameter is obtained which can be solved to give s as a function of the wave number.

$$s = U_s k \pm[(\sigma k^3/\rho_l - k^2U_s^2\rho_g/\rho_l)/\coth(kh_o)]^{1/2} \quad (A27)$$

ACKNOWLEDGEMENTS

The authors wish to acknowledge Dr. Terry Adams and Dr. Jeff Lindsay for their helpful discussion and insight. We would also like to recognize the financial support of the member companies of the Institute of Paper Science and Technology and the U.S. Department of Energy (contract No. FC02-88CE40839). Thanks also to Smith Meter Inc. and Fluid Flow of Georgia, Inc. for the donation of a mass flow meter. Portions of this work were used by T.M.S. as partial fulfillment of the requirements for the Ph.D. degree at the Institute of Paper Science and Technology.

REFERENCES

1. Spielbauer, T.M.; Adams, T.N.; Monacelli, J.E.; Bailey, R.T. Droplet Size Distribution of Black Liquor Sprays, CPPA Int. Chem. Rec. Conf. Ottawa:119-25(April 3-6, 1989).

2. Bennington, C.P.J.; Kerekes, R.J. The Effect of Temperature on Drop Size of Black Liquor Sprays, J. Pulp and Paper Sci., 12(6):J181-6(Nov., 1986).

3. Taylor, Sir Geoffrey Oblique Impact of a Jet on a Plane Surface, Phil. Trans. Roy. Soc. London A, (260):96-100(1966).

4. Clark, C.J.; Dombrowski, N. The Dynamics of the Rim of a Fan Spray Sheet, Chem. Eng. Sci., 26:1949-51(1971).

5 Obuskovic, N.; Adams, T.N. Fluid Sheet Thickness and Velocity at the Tip of a Black Liquor Splashplate Nozzle, AIChE 1989 Annual Meeting, San Francisco, CA, (Nov. 5-10, 1989).

6. Taylor, Sir Geoffrey The Dynamics of Thin Sheets of Fluid; I: Water Bells, Proc. Roy. Soc. London A(253):289-95(Dec., 1959).

7. Dombrowski, N.; Fraser, R.P. A Photographic Investigation into the Disintegration of Liquid Sheets, Phil. Trans. Roy. Soc. London, 247A:101-30(1954).

8. Panton, R.L. Incompressible Flow, John Wiley and Sons, Inc.:675-9(1984).

9. Dombrowski, N.; Johns, W.R. The Aerodynamic Instability of Viscous Liquid Sheets, Chem. Eng. Sci., 18:203-14(1963).

10 Hagerty, W.W.; Shea, J.F. A Study of the Stability of Plane Fluid Sheets, J. of Applied Mechanics, 509-14(Dec., 1955).

11. Squire, H.B. Investigation of the Instability of a Moving Liquid Film, Brit. J. of Applied Physics, 4:167-9(June, 1953).

12. Fraser, R.P.; Eisenklam, P.; Dombrowski, N.; Hasson, D. Drop Formation from Rapidly Moving Liquid Sheets, AIChE Journal, 8(5):672-80(Nov., 1962).

13. Adamson, A.W. Physical Chemistry of Surfaces, 2nd Edition, John Wiley & Sons, Inc.:6(1967).

14. Crapper, G.D.; Dombrowski, N.; Jepson, W.P. Wave Growth on Thin Sheets of Non-Newtonian Liquids, Proc. R. Soc. London A, 342:225-36(1975).

15. York, J.L.; Stubbs, H.E.; Tek, M.R. The Mechanism of Disintegration of Liquid Sheets, Trans. ASME:1279-86(Oct., 1953).

16. Weihs, D. Stability of Thin, Radially Moving Liquid Sheets, J. Fluid Mech., 87(2):289-98(1978).

17 Crapper, G.D; Dombrowski, N.; Pyott, G.A.D. Kelvin-Helmholtz Wave Growth on Cylindrical Sheets, J. Fluid Mech., 68(3):497-502(1975).

18. Taylor, G.I.; Michael, D.H. On Making Holes in a Sheet of Fluid, J. Fluid Mech., 58(4):625-39(1973).

19 Rayleigh, Lord J.W.S. The Theory of Sound Vol.2, Dover Publications, NY:343-75(1945) (republication of 1896 edition).

20. Weber, C. Zum Zerfall eines Flussigkeitsstrahles, Z. Agnew. Math. und Mech., 11(2):136-54(April, 1931).

21. Lafrance, P. Nonlinear Breakup of a Laminar Liquid Jet, The Physics of Fluids, 18(4):428-32(April, 1975).

22. Chaudhary, K.C.; Redekopp, L.G. The Nonlinear Capillary Instability of a Liquid Jet, J. Fluid Mech., 96(2):257-74(1980).

23. Torpey, P.A. A Nonlinear Theory for Describing the Propagation of Disturbances on a Capillary Jet, Phys. Fluids A., 1(4):661-71(April, 1989).

24. Yuen, M. Non-linear Capillary Instability of a Liquid Jet, J. Fluid Mech., 33(1):151-63(1968).

25. Weihs, D.; Frankel, I. Equilibrium Shape and Stability of a Liquid Cylinder in Cross Flow at Low Weber Numbers, J. Fluid Mech., 116:393-409(1982).

26. Spielbauer, T.M.; Adams, T.N. Flow and Pressure Drop Characteristics of Black Liquor Nozzles, AIChE Annual Meeting, San Francisco, CA(Nov., 1989).

27. Taylor, G.I. The Dynamics of Thin Sheets of Fluid; III: Disintegration of Fluid Sheets, Proc. Roy. Soc. London A 253:313-21(1959).

28. Taylor, G.I. The Dynamics of Thin Sheets of Fluids; II: Waves on Fluid Sheets, Proc. Roy. Soc. London A 253:296-312(1959).

29. Huang, J.C.P. The Break-up of Axisymmetric Liquid Sheets, J. Fluid Mech. 43(2):305-19(1970).